IEEE Access
Multidisciplinary | Rapid Review | Open Access Journal

Received July 8, 2019, accepted July 28, 2019, date of publication August 1, 2019, date of current version September 9, 2019.

Digital Object Identifier 10.1109/ACCESS.2019.2932331

Four Ports Double Y-Shaped Ultra-Wideband Magneto-Photonic Crystals Circulator for 5G Communication System

YONG WANG[1,3], DENGGUO ZHANG[2], BIAOGANG XU[3], ZHENG DONG[2], XUANKE ZENG[1,3], JIHONG PEI[2], (Member, IEEE), SHIXIANG XU[1], AND QUAN XUE[4,5], (Fellow, IEEE)

[1]Shenzhen Key Laboratory of Micro-Nano Photonic Information Technology, College of Physics and Optoelectronic Engineering, Shenzhen University, Shenzhen 518060, China
[2]College of Electronics and Information Technology, Shenzhen University, Shenzhen 518060, China
[3]College of Physics and Optoelectronic Engineering, Shenzhen University, Shenzhen 518060, China
[4]School of Electronic and Information Engineering, South China University of Technology, Guangzhou 510000, China
[5]Department of Electrical Engineering, City University of Hong Kong, Hong Kong 999077

Corresponding authors: Dengguo Zhang (dgzhang@szu.edu.cn) and Shixiang Xu (shxxu@szu.edu.cn)

This work was supported in part by the National Natural Science Foundations of China under Grant 61775142 and Grant 61171006, in part by the China Postdoctoral Science Foundation under Grant 2019M653028 and Grant 2017M612726, and in part by the Specialized Research Fund for Shenzhen Strategic Emerging Industries Development under Grant JCYJ20170412105812811.

ABSTRACT This paper presents a novel four ports double Y-shaped photonic crystals circulator with ultra-wide bandwidth in 5G millimeter wave band. Its insertion loss can be designed as low as 0.38 dB at 26.10 GHz while its optimal isolation is up to 74.86 dB at 25.00 GHz. The circulator keeps its isolation above 20 dB from 21.80 to 29.04 GHz. Our simulations also show the relative bandwidth can be effectively broadened to be 28.48% through adding an impedance matching transformer composed of four triangular metal pedestals. We confirmed our theoretical results with a circulator sample made of a triangular-lattice Al_2O_3 ceramic rod array and ferrite posts. The minimal measured isolation and insertion loss have reach 47.61 dB and 0.80 dB at 25.55 GHz and 26.10 GHz, respectively. The operating spectral region of our sample covers from 24.08 to 28.23 GHz (the relative bandwidth is 15.87%), which is about seven times higher than the best simulated result of 2.5% and fifteen times higher than 1.07%, the published experimental value. Our experimental results are well matched with the numerical simulations. The low loss, high isolation and ultra-wideband characteristics demonstrate that our photonic crystal circulator has potential applications in 5G communication systems.

INDEX TERMS Photonic crystals, circulator, ultra-wideband, millimeter wave, 5G.

I. INTRODUCTION

Usually circulators are nonreciprocal devices used in communication systems. They isolate multiple reflections between elements or modules, thereby ameliorate tolerance for manufacturing defects and environmental fluctuations [1]–[4], especially, as duplexers in radar communication system [5]–[8].

Photonic crystals (PCs) have attracted considerable attention due to their abilities to control photonic motions [9], [10]. Their high integration makes them be one of the promising candidates for the future optical communications. Because of their unique photonic band gap (PBG) and photonic localization, PCs can be used to develop circulators for high density optical integration. In recent years, PCs circulators have been vigorously studied due to their great flexibilities in the designs [11]–[16]. In the optical frequency band, a three-port ''windmill'' shaped PCs circulator was first proposed and designed by introducing air hole array in bismuth iron garnet (BIG), whose bandwidth for 30 dB isolation at 1550 nm is estimated to be 12.6 GHz [11]. A type of carefully designed magneto-photonic crystals (MPC) cavity was carefully designed to realize a W-shaped circulator with optimal isolation of 40 dB also at 1550 nm band, but this circulator's relative bandwidth is only about 0.05% [12]. In engineering, bandwidth is usually as important as the isolation and

The associate editor coordinating the review of this article and approving it for publication was Dušan Grujić.

insertion loss for circulators. However, all the bandwidths of the reported MPC circulators above are all less than 0.1%. A magnetically tunable circulator with high isolation of 65.2 dB is designed at 0.2 THz by using two-dimensional (2-D) rods array [13], which has its relative bandwidth up to about 2.5%. For microwave and photon communication system, a Y-shaped [14] and a cross-shaped [15] MPC circulators also encounter with narrow bandwidth in X-band. From above, it is evident that PCs have great flexibilities in the design of circulators at some different frequency bands, but fail to provide broad bandwidth for MPC circulators until now.

As we know, 5G communication devices and systems have drawn considerable attention and been widely studied due to the advantages of high rate and wide bandwidth [17]–[23]. The 5G millimeter wave communication network right now will work within the range from 24 to 28 GHz in the majority of countries and region in the world, *e.g.* America (27.5∼28.35 GHz), China (24.75∼27.5 GHz), Europe (24.25∼27.5 GHz), Japan (28 GHz), Korea (28 GHz) and Australia (26 GHz). Accordingly, to develop MPC circulators with broad bandwidth is very interesting at 5G frequency region, in spite of great challenge.

In this paper, a novel four ports double Y-shaped MPC circulator with ultra-wideband is proposed based on gyromagnetic ferrite posts and the numerical optimization of photonic crystal waveguide (PCW), and first fabricated in 5G millimeter waveband. Through the numerical simulation on the relationship between the transmission efficiency of the PCW with its size in three-dimensional (3-D) model, the optimal PCW structure with high transmission efficiency 90.78% is designed and validated at K-Ka band. With the high transmission PCW, the measured insertion loss of the MPC circulator can greatly reduce to 0.80 dB at the central frequency 26.10 GHz in corresponding experiments here. Through combining the band broadening technique of waveguide circulator with the PCs circulator technology, our circulator sample has a wide bandwidth from 24.08 to 28.23 GHz (the relative bandwidth is 15.87%), which is about seven times higher than the best simulated result of 2.5% in [13] and fifteen times higher than the experimental result of 1.07% in [14]. The low loss and easy integration demonstrate that the designed scheme of our MPC circulator not only can reduce light intensity to avoid nonlinear effect for integrated optical circuit if in optical waveband, but also has potential applications in 5G communication systems due to its ultra-wideband characteristic at 24 to 28 GHz band.

II. NUMERICAL CALCULATION RESULTS

A. DESIGN OF DOUBLE Y-SHAPED MPC CIRCULATOR

As shown in Fig. 1, our MPC circulator consist of PCW, which includes a pair of the rhombic metal waveguide (blue) to fix the 2-dimentional (2-D) triangle lattice photonic crystals (TLPCs) (white). There are four ports at the centers of the four sides of rhombic PCW, which connect with the four ends of the double Y-shaped passage.

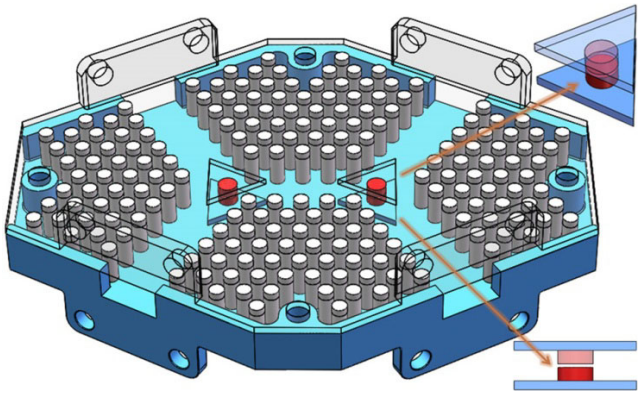

FIGURE 1. Design of four ports double Y-shaped MPC circulator.

There are 4 Ni-Zn ferrite posts (red) in our MPC circulator, where each two ferrites are situated at the central position of the two junctions in the double Y-shaped passage. The detail diagrams in the upper right and lower right corner of Fig. 1 show that the two ferrite posts distributed up and down in each ferrite area. In order to distinguish the tiny distance of the upper and lower ferrite posts, we make a transparent display of the upper post. Here, in order for the external matching broadening method (EMBM) [24], [25], every ferrite post is equipped with a triangular metal pedestal to realize impedance matching, which is widely used for the band broadening of waveguide circulators. The ferrite post driven by an external magnetic field not only acts as a resonant cavity, but also supplies the needed degree Faraday rotation. The radius and height of the ferrite posts are designed by equation 5 in section C, which depend on the operating frequency of the circulator. Four flange interfaces are set at the four ports for convenience to connect with the test equipment.

B. HIGH TRANSMISSION PCW WITH ULTRA-WIDE PBG

In order to realize the ultra-wideband MPC circulator with low insertion loss, a high transmission PCW with ultra-wide PBG is needed to design firstly. Through the numerical simulation on the relationship between the transmission efficiency of the PCW with its size in 3-D model, the optimal PCW structure is designed in this section and the construction is shown in Fig. 2.

As shown in Fig. 2(a), our PCW includes two TLPCs formed by Al_2O_3 ceramic rods arrays, which are fixed with the upper and lower metal plates. The distance of the two arrays is marked by the width w, as shown in Fig. 2(b). The lattice constant A of the TLPCs is 3.5 mm, while the radius r_0 and permittivity of the Al_2O_3rods are 1 mm and 9.2, respectively. There are four flange interfaces at the centers of the four sides of the PCW, including ports 1 and 3 which are used to measure the transmission efficiency of the PCW, while the other two ports 2 and 4 are used to measure the reflection coefficient of the TLPCs. The ceramic rod arrays positioned with high accuracy allows the TLPCs to guarantee the PBG characteristics.

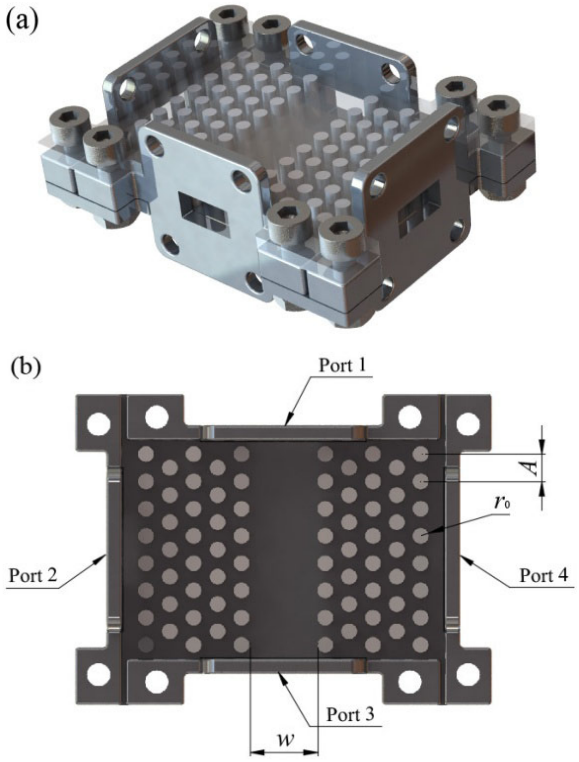

FIGURE 2. (a) PCW with triangular lattice rods arrays; (b) the sectional view of the PCW.

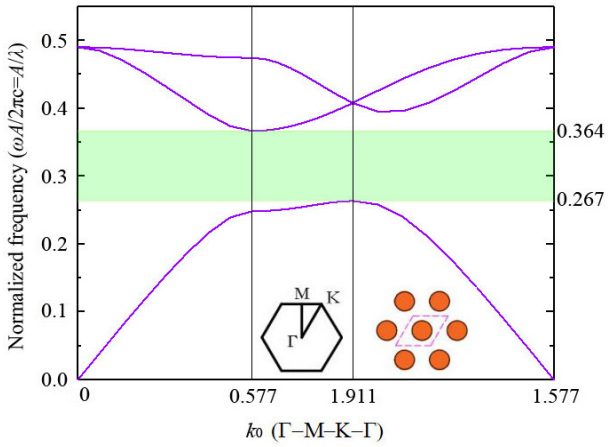

FIGURE 3. The TE band structures of the TLPCs.

Theoretically, the PBG of the PCs determines the frequency of the electromagnetic waves that can be transmitted in the PCW. We confirm the PBG by analyzing the band structure of the TLPCs, which is formed by Al_2O_3 rods without any defect. With the mentioned parameters of the TLPCs above, its band structure is calculated by plane wave expansion method. In Fig. 3, the broad PBG is only for TE modes with its normalized frequency from 0.267 ($2\pi c/A$) to 0.364 ($2\pi c/A$), where c is the speed of the light. When the distance A of the two adjacent Al_2O_3 rods, called lattice constant, is 3.5 mm, the normalized frequency region corresponds a range

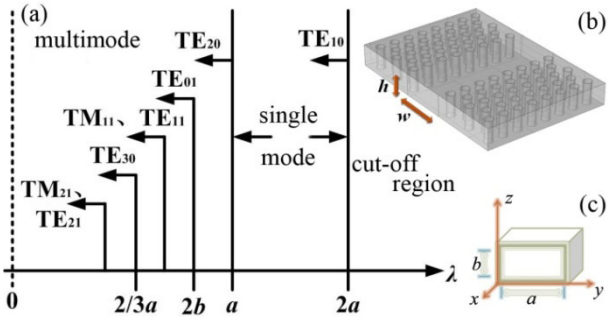

FIGURE 4. (a) Modes in rectangular waveguide; (2) PCW with 3-D model; (c) Diagram of rectangular waveguide.

from 22.89 to 31.20 GHz. In principle, the TLPCs forbid the propagation of electromagnetic waves within these PBG frequency ranges but the waves can be confined to propagate in the PCW due to the photonic localization effect.

In millimeter wave band, the relationship between the transmission mode of a rectangular metal waveguide and its sizes is shown as in Fig. 4(a). For the size $a \times b$ of rectangular waveguide given in Fig. 4(c), it has a cutoff wavelength λ_c for TE_{mn} or TM_{mn} modes described as following:

$$\lambda_c = \frac{2}{\sqrt{\left(\frac{m}{a}\right)^2 + \left(\frac{n}{b}\right)^2}}. \tag{1}$$

It shows that every normal wave represented for TE_{mn} or TM_{mn} modes has a corresponding cutoff wavelength λ_c. The input electromagnetic wave with wavelength $\lambda_0 < \lambda_c$ can propagate in the waveguide. Fig. 4(a) shows that the rectangular waveguide operates in a single-mode state only when the wavelength of incident electromagnetic wave satisfies $a < \lambda_0 < 2a$. Here, it is also necessary to avoid the higher electromagnetic mode TE_{01} ($\lambda_0 > 2b$), thereby to ensure that there is only the captain mode TE_{10} in the waveguide.

Obviously, the designed PCW with height h and width w as shown in Fig. 4(b) is similar to rectangular waveguide with height b and width a as shown in Fig. 4(c). Similarly, the condition ($w < \lambda_0 < 2w$ and $\lambda_0 > 2h$) of single mode transmission must be satisfied in order to realize the single mode transmission in the PCW. If $w = 2h$, the transmission efficiencies' variation of the PCW with its sizes can be simulated at the interested frequency region from 24 to 28 GHz, as shown in Fig. 5. In order to ensure that all electromagnetic waves in the frequency region meet the conditions of single mode propagation ($w < \lambda_0 < 2w$), the range of width for the PCW is calculated to be 6.25 mm $< w <$ 10.7 mm ($w = 2h$).

As shown in Fig. 5, the transmission efficiency of the PCW increases with its width w and height h. When $w > 6.9$ mm, all the transmission efficiencies of the electromagnetic waves with frequencies from 24 to 28 GHz are above -1dB (about 79.43%). When $w > 7.5$ mm, the electromagnetic wave' transmission efficiency at 26 GHz is greater than those at 24, 25 and 28 GHz, but smaller than that at 27 GHz. When $w > 8.2$ mm, the transmission efficiency of the electromagnetic wave at 26 GHz is greater than those at other frequency

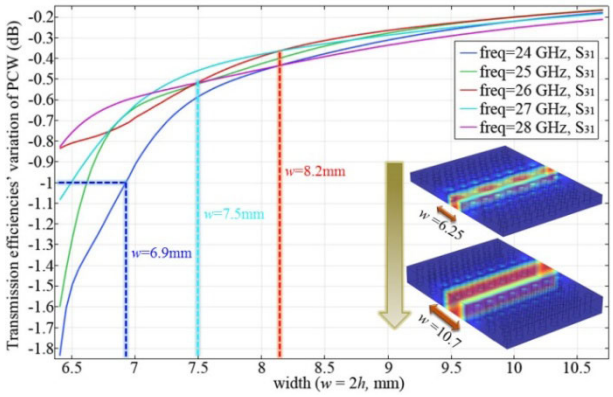

FIGURE 5. The transmission efficiencies' variation of PCW with its sizes at different frequencies.

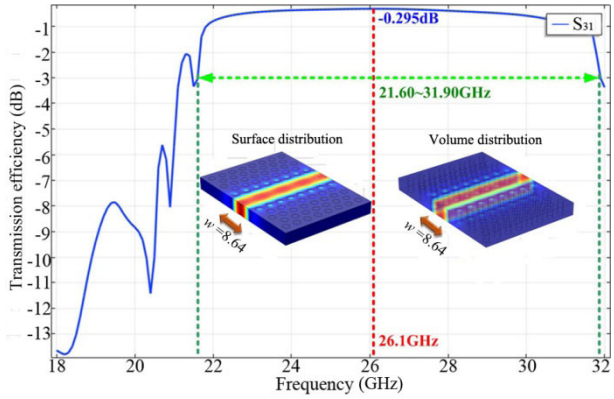

FIGURE 6. The transmission efficiency's variation of PCW with frequency when $w = 2h = 8.64$ mm.

bands. Therefore, the size of the PCW can be reasonably designed in engineering according to the above relations when the operating frequency band is given in advance.

As we know, the size of WR34 is 8.64×4.32 mm^2, which is the current standard rectangular waveguide's size at K-Ka band. Accordingly, the PCW is designed in accordance with WR34 for easy measurement and comparison. The transmission efficiency's variation of the designed PCW with frequency is simulated as shown in Fig. 6. The inserting two figures of electromagnetic field distribution in the waveguide are surface distribution (left) and volume distribution (right) respectively. The optimal transmission efficiency is up to 92.43% (−0.295dB) at the central frequency of 26.10 GHz. From 21.60 GHz to 31.90 GHz, the PCW keeps its transmission efficiency above −3 dB. The relative bandwidth is about 38.50%. These data show that the designed PCW has ultra-wideband and high transmission characteristics.

In Fig. 7, the transmission characteristics of the PCW and the electromagnetic field propagation with different frequencies are simulated by finite element method (FEM). The calculated region is divided into 100,000 grid cells and the boundary condition is set for Perfect Electric Conductor. The numerical results show that the electromagnetic waves

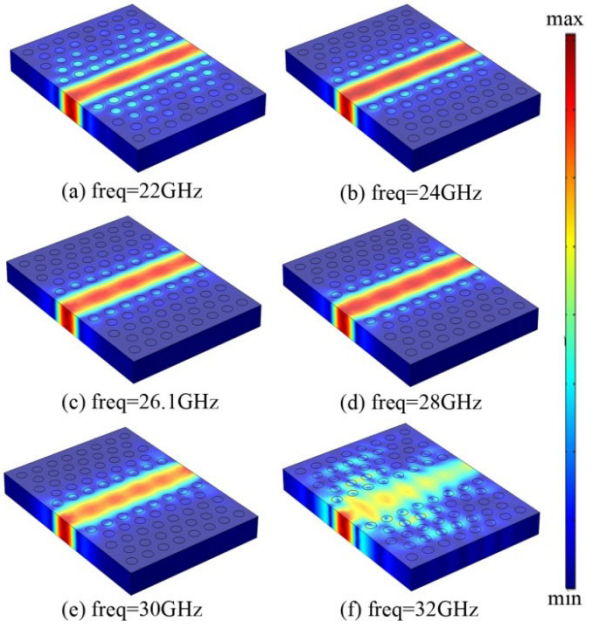

FIGURE 7. Transmission characteristics of the PCW and the electromagnetic field propagation with different frequencies.

launched from Port 1 are transmitted stably to Port 3 in the PCW at the frequencies of 24, 26.1, 28 and 30 GHz, as shown in Figs. 7(b)–(e). The partial energy of the electromagnetic waves spreads into the TLPCs at the frequencies of 22 and 32 GHz with the optical local effect of the PCW decaying when the electromagnetic waves' frequency is near the boundary of the PBG, as shown in Figs. 7(a) and 7(f).

C. PROPERTIES OF THE GYROMAGNETIC FERRITE

The propagation direction of the electromagnetic waves is deflected in the circulator, which is mainly attributed to the gyromagnetic properties of the central ferrite posts. In the millimeter wave band, the gyromagnetic property of ferrite post magnetized in z-direction can be represented with the permeability tensor [26]:

$$[\mu_r] = \mu_0 \begin{bmatrix} \mu & j\kappa & 0 \\ -j\kappa & \mu & 0 \\ 0 & 0 & 1 \end{bmatrix}. \tag{2}$$

The elements μ and κ can be expressed as

$$\mu = 1 + \frac{\omega_0 \omega_m}{\omega_0^2 - \omega^2} \tag{3}$$

and

$$\kappa = \frac{\omega \omega_m}{\omega_0^2 - \omega^2}. \tag{4}$$

Here $\omega_0 = \mu_0 \gamma H_0$ and $\omega_m = \mu_0 \gamma M_s$. H_0 is the bias magnetic field, while $\gamma = 1.759 \times 10^{11}$ C/kg and $M_s = 2.39 \times 10^5$ A/m, which stand for gyromagnetic ratio and saturation magnetization, respectively.

Usually, the central frequency and bandwidth of a ferrite circulator are designed by following formula [27]:

$$R = x \Big/ \left\{ \left(2\pi f_0 \sqrt{\varepsilon_r}/299.793\right)^2 - \left[\left(\pi/l_f\right) \times 1.5\right]^2 \right\}^{1/2}, \quad (5)$$

which describes the approximate relationship between the size, relatively permittivity and frequency of a ferrite cylindrical resonator. Here, R is the radius of the central ferrite with height l_f, while $\varepsilon_r = 13.5$ is the Ni-Zn ferrite's relatively permittivity. x, about 2.2 here, is a compromise value in [27], to insure a appropriate size of the central ferrite posts for the double Y-shaped passage of circulator. In that way, the size of the central ferrite posts can be designed according to a given central frequency. The operating frequency of our circulator is preferentially designed to be 26.10 GHz that is in conformance with central frequency of the PCW in section B. According to eqn. 5, the ferrite post's radius R is computed to be 1.6 mm with the height $l_f = 3.2$ mm.

D. BAND BROADENING OF MPC CIRCULATOR

In this section, the bandwidth of the MPC circulator is numerically studied based on the ultra-wideband PCW and gyromagnetic ferrite posts described in the previous sections. The structural parameters of the PCW and ferrite posts are same with those mentioned above. The numerical model of the MPC circulator is designed as shown in Fig. 8(a). In order to broaden the bandwidth of the designed MPC circulator, four triangular aluminum pedestals are put at the center of the junctions in the double Y-shaped PCW to constitute an impedance matching transformer as shown in the transparent view. The matching transformer with appropriate size and position can realize simultaneous matching of all ports for the circulator. This method of placing metal pedestals with symmetrical shape in the symmetrical position of the waveguide's junctions is usually used in waveguide circulator for band broadening [24], [25], called EMBM mentioned above. Through combining the band broadening technique of waveguide circulator with the PCs circulator technology, the relative bandwidth of our designed MPC circulator is broadened to be 28.48% in the numerical simulation.

As shown in Figs. 8(b) and 8(c), the function and transmission characteristics of the MPC circulator are calculated by FEM based on Maxwell equation with permeability tensor $[\mu_r]$ like [13], as follows:

$$\varepsilon^{-1} \cdot \nabla \times \left([\mu_r]^{-1} \cdot \nabla \times \vec{E} \right) = \omega^2 / c^2 \cdot \vec{E}, \quad (6)$$

where ε is a constant, while ω is the frequency of incident electromagnetic wave and $\vec{E}$ is electric field intensity. The computing area includes about 1.06 million grid cells, which is surrounded with scattering boundary condition (SBC). In Fig. 8(a), the four ports of the designed circulator are expressed as Port 1, 2, 3 and 4. When Port 1 acts as the input port, the isolation and insertion loss for the designed circulator are calculated at the frequency region from 18 to 32 GHz as shown in Fig. 9(a). The variation of insertion loss from port 1 to port 2 for the MPC circulator with frequency

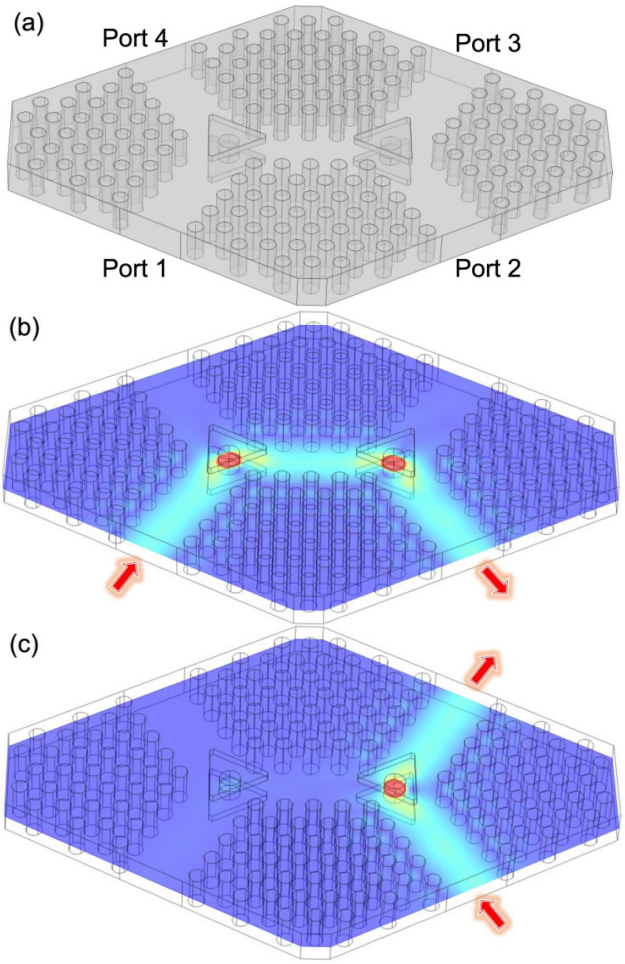

FIGURE 8. (a) The numerical model of the MPC circulator; (b) Electromagnetic field propagation from port 1 to port 2 in circulator; (c) Electromagnetic field propagation from port 2 to port 3 in circulator.

is represent as S_{21}, which is low to 0.42 dB at 26.10 GHz. For port 3 to port 1, the optimal isolation is 46.14 dB at 24.71 GHz and the bandwidth of the circulator cover from 23.66 to 28.63 GHz with its isolation below 20 dB. For port 4 to port 1, the optimal isolation is 48.60 dB at 26.40 GHz and the bandwidth of the circulator is from 24.40 to 27.28 GHz.

The distribution situation of electromagnetic wave's power in the circulator is simulated at 26.10 GHz, as shown in Fig. 8(b). It is obvious that the propagation direction of signal arises a 120° rotation at the first ferrite region and rotates 120° again at the second ferrite region with the action of the bias magnetic field $H_0 = 376.99$ mT. So the function of the double Y-shaped MPC circulator is realized that the signal is transmitted stably from port 1 to port 2 while port 3 and port 4 are isolated.

When the electromagnetic waves are launched from Port 2 and circularly propagate to the Port 3, the other two posts 1 and 4 are isolated as shown in Fig. 8(c). In Fig. 9(b), the isolations of the MPC circulator reach 74.86 dB at 25.10 GHz for port 1 to port 2 and 43.10 dB at 24.80 GHz for port 4 to port 2, respectively. The insertion loss of the circulator is low to 0.38 dB at the central frequency of 26.10 GHz

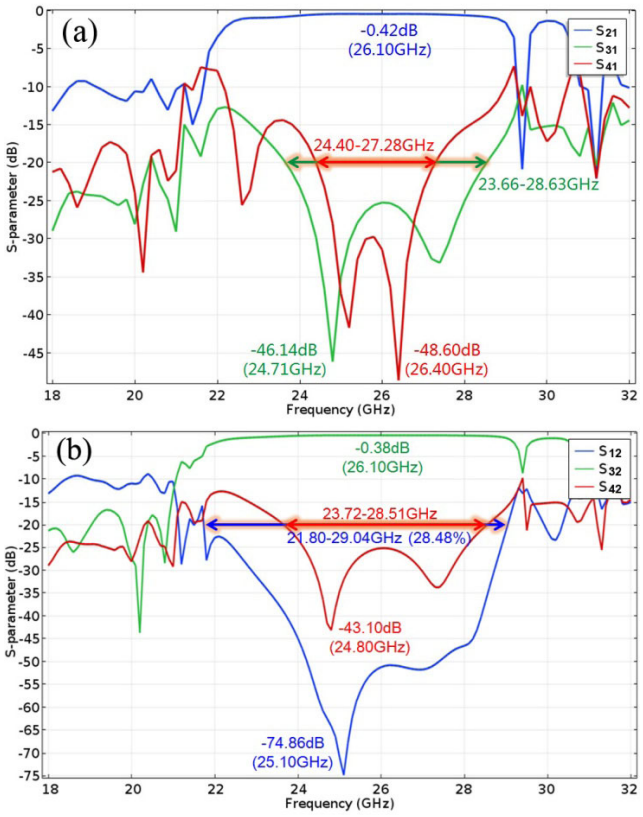

FIGURE 9. (a) Variation of external characteristic parameters with frequency for port 1 acting input port; (b) Variation of external characteristic parameters with frequency for port 2 acting input port.

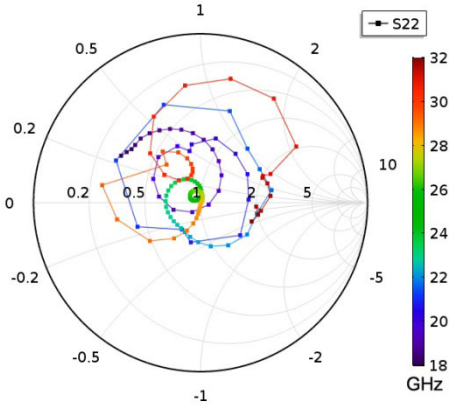

FIGURE 10. Reflection characteristic of port 2 for the MPC circulator.

and the electromagnetic wave's distribution situation is also simulated as shown in Fig. 8(c).

Significantly, the relative bandwidth of the circulator is broadening to be 28.48% with frequency region from 21.80 to 29.04 GHz in the numerical simulation as shown in Fig. 9(b), which demonstrate that our designed MPC circulator's performance can reach the ultra-wideband level. Due to placing suitable metal pedestals described above in the double Y-shaped waveguide's junctions can realize the perfect matching for the MPC circulator. When the external circle's radius and thickness of the triangular pedestals are optimized to 5 mm and 0.9 mm respectively, the port 2 of the circulator has almost no reflection at 26.10 GHz as shown in Fig. 10. The numerical results show that the signals propagate circularly and stably in the designed circulator which has ultra-wideband performance.

E. QUANTITATIVE ANALYSIS WITH THE BANDWIDTH

Taking the second transmission path in Fig.8(b) as an example, the bandwidth of the circulator changes obviously when the radius of the central ferrite post is different, as shown in Figs. 11 and 12. When the radius of the central ferrite post slightly deviated from 1.60 mm to 1.58 or 1.62 mm, the three curves of insertion loss for the circulator are basically coinciding with each other but there is a slight movement for the bandwidth, as shown in Fig. 11. As the radius R decreases to be 1.58 mm, the curves (S_{42} and S_{12}) of spectral isolation assume a blue shift. The frequency regions of bandwidth (isolation above 20 dB) shift to be 24.00 to 28.80 GHz (S_{42}) and 21.80 to 29.00 GHz (S_{12}), while the relative bandwidths have barely changed.

As the radius R increases to be 1.62 mm, the curves (S_{42} and S_{12}) of spectral isolation assume a red shift. The frequency regions of bandwidth (isolation above 20 dB) shift to be 23.50 to 28.20 GHz (S_{42}) and 21.80 to 29.00 GHz (S_{12}), while the relative bandwidths almost no change.

When the radius of the central ferrite post deviates from 1.60 mm to 1.50 or 1.70 mm, the variation trend of the three curves for insertion loss (S_{32}) are still consistent with each other, as shown in Fig. 12, but the curves of the circulator's isolation assume biggish change. As the radius R decreases to be 1.50 mm or increases to be 1.70 mm, the isolation's blue or red shift still appears and all the isolations have a sharp degradation. The isolations between port 4 and port 2 (S_{42}) are even below 20 dB in our interesting frequency region of 24.00 to 28.00 GHz, thus there has no bandwidth for the designed circulator.

When the radius R_1 of the triangle pedestals deviates from 5.00 mm to 4.50 or 5.50 mm, the five curves of insertion loss (S_{32}) for the circulator are still coinciding with each other, as shown in Fig. 13(a). Whether the radius R_1 decreases or increases, all the circulator's isolations become worse and the bandwidth narrow down, while the reflection of the input port (S_{22}) gradually increase shown in Fig. 13(b). This shows that the circulator's impedance matching deteriorate as the radius of the pedestals deviates from 5.00 mm. When R_1 is 4.50 mm or 5.50 mm, the isolation between port 4 and port 2 (S_{42}) is even below 20 dB at some frequencies. Observingly, there has no red or blue shift of the spectral isolation when the radius of the triangle pedestals changes.

In discussion, on the one hand, the radius of the central ferrite posts obviously affects the bandwidth and isolation of the designed circulator in above numerical simulation. The blue or red shift of the bandwidth perfectly accord with eqn.

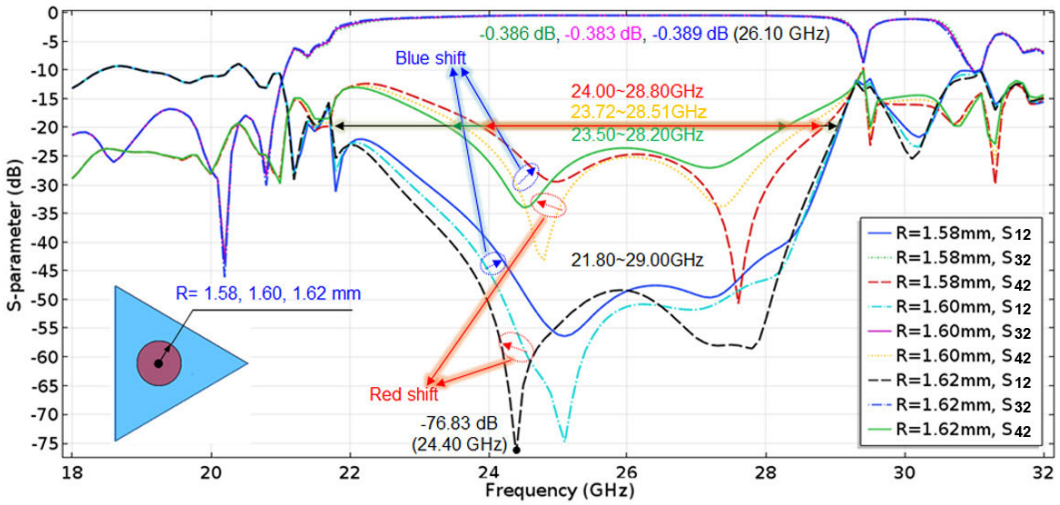

FIGURE 11. The bandwidth of the MPC circulator with the slightly changing radius of the central ferrite posts at 1.58 mm, 1.60 mm, 1.62 mm.

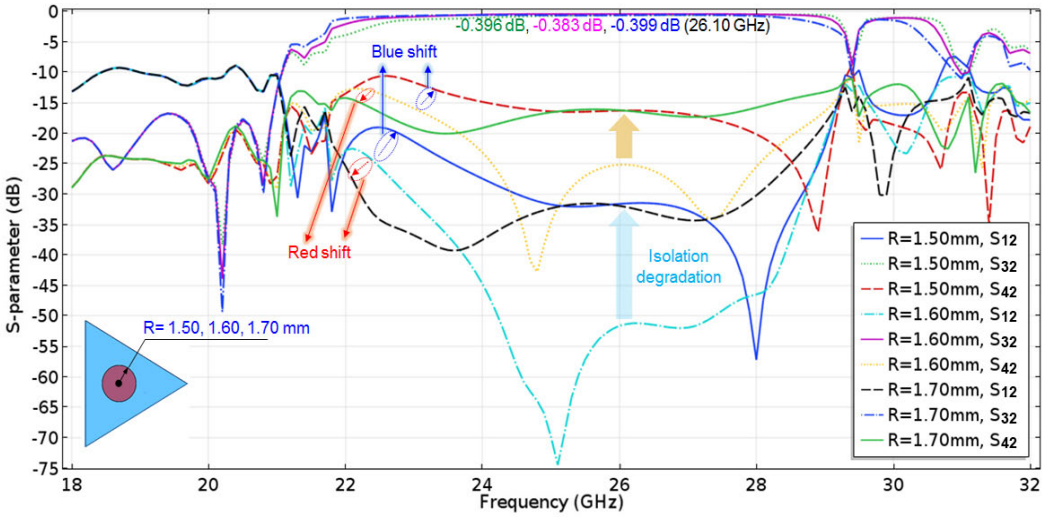

FIGURE 12. The bandwidth of the MPC circulator with the obviously changing radius of the central ferrite posts at 1.50 mm, 1.60 mm, 1.70 mm.

(5) which describes the relationship between the resonance frequency and the size of the cylindrical resonator in a ferrite circulator. Moreover, the size of the ferrite posts also affects the circulator's impedance matching through observing the isolations' sharp degradation in Fig. 12. On the other hand, we observe that the changing radius of the triangle pedestals also has great influence on the isolation and bandwidth, but there has no red or blue shift of the spectral isolation. It means that the pedestals' function is mainly impedance matching but almost unaffected the resonance frequency for the circulator. Additionally, the size of the PCs waveguide obviously affect the transmission efficiency of PCs transmission line, whose optimal size has been used in the design of the magneto-photonic crystal circulator through the detailed analysis in section B above.

III. EXPERIMENTAL VERIFICATIONS

A. EXPERIMANTAL VERIFICATIONS OF PBG AND PCW

Before verifying the MPC circulator, the designed PCW with ultra-wide PBG needs to be verified by experiments firstly. In order to validate the aforementioned numerical results of TLPCs and PCW, the experiments are carried out at K-Ka band within the frequency range of 18∼32 GHz by using an Agilent E8361C vector network analyzer. The detailed structural parameters of the PCW sample are given in section B above, as shown in Fig. 2. The size of flange ports is 8.64×4.32 mm^2. The rubber plate absorbing materials with thickness 0.8mm are set around the Al_2O_3 rods arrays to absorb noise in the rectangular aluminous waveguide. The normal incident reflection coefficient of the absorbing materials is less than −20 dB from 18 to 35 GHz.

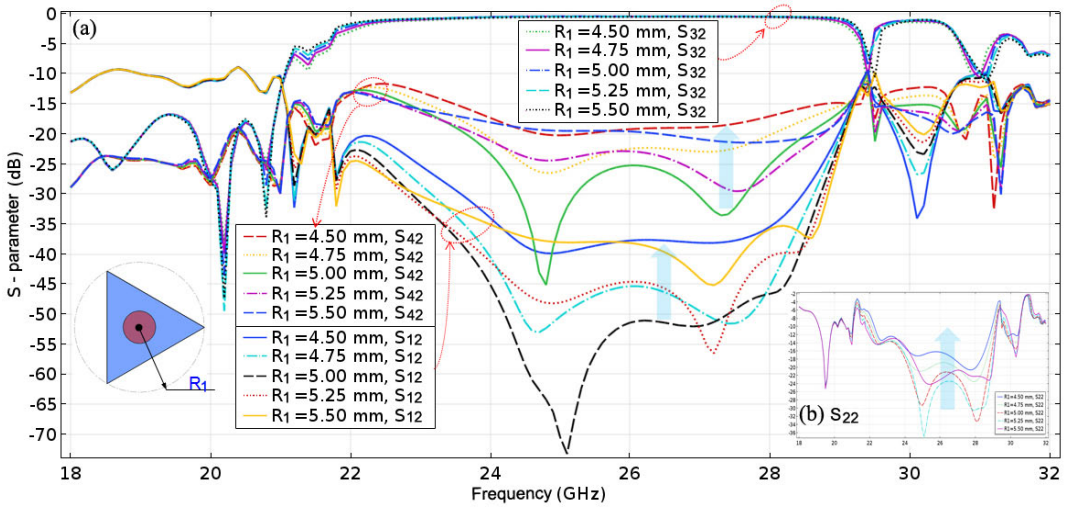

FIGURE 13. The external properties of the MPC circulator with the changing radius of the triangle pedestals from 4.50 mm to 5.50 mm.

Figs. 14(a), (c) and (e) present the experimental setup for measuring the loss of the Sub-Miniature Version A (SMA) connectors and waveguide to coaxial converters, the reflection characteristics of the TLPCs and the transmission efficiency of the PCW, respectively. The PCs samples and the vector network analyzer are connected through two waveguides to coaxial converters and a pair of SMA connectors. Correspondingly, the experimental results are shown in Figs. 14(b), (d), (f), respectively.

In the experiments, the parameter S_{11} represents logarithmic value of the ratio of the reflected power to the input power of the Port 1. And the parameter S_{21} represents logarithmic value of the ratio of the transmission power of the Port 2 from the input power of the Port 1. Similarly, S_{12} and S_{22} represent the transmission and reflection characteristics of the Port 2. In the classical measurement of the network analyzer, the S parameters are respectively expressed as follows:

$$S_{11} = 10\lg(P_{R1}/P_1), \tag{7}$$
$$S_{21} = 10\lg(P_{21}/P_1), \tag{8}$$
$$S_{12} = 10\lg(P_{12}/P_2), \tag{9}$$
$$S_{22} = 10\lg(P_{R2}/P_2), \tag{10}$$

where, P_1 and P_2 are the input power of the Port 1 and 2. P_{R1} and P_{R2} are the reflected power of Port 1 and 2. P_{21} is the transmission power from Port 1 to Port 2, and P_{12} is the transmission power from Port 2 to Port 1.

When the insertion loss of the electric cable is ignored, the loss α_1 of the SMA connectors and waveguide to coaxial converters shall be

$$\alpha_1 = S_{21} \approx S_{12} = 10\lg\left(P_{21/12}/P_1\right). \tag{11}$$

As shown in Fig. 14(b), α_1 has been measured with the setup in Fig. 14(a), which are -0.57 dB, -0.50 dB or -0.51 dB at 26.10 GHz, 23.39 GHz or 31.23 GHz.

The reflection coefficient β of the PCs is expressed as follows:

$$\text{lolg}\,\beta = S_{11/22} - \alpha_1/2 = 10\lg(P_{R12}/P_{12}) - \alpha_1/2, \tag{12}$$

which is 91.41% (-0.96dB + 0.57dB) at 26.10 GHz measured in Fig. 14(c) as shown in Fig. 14(d). The measured PBG in the region from 21.99 to 29.15 GHz ($\beta > -3$dB) matches well with the numerical result in section B above in Fig. 3.

Furthermore, the transmission efficiency η of the PCW is

$$\eta = S_{21/12} - \alpha_1 = 10\lg\left(P_{21/12}/P_{1/2}\right) - \alpha_1, \tag{13}$$

whose variation with frequency as shown in Fig. 14(f). The experimental results show that: at the central frequency of 26.10 GHz, the measured η is up to 90.78% (-0.42 dB); while the bandwidth ($\eta > -3$dB) is about 7.84 GHz with frequency region from 23.39 to 31.23 GHz that matches well with the numerical calculations in Fig. 6. The confirmatory experiments demonstrate that the designed PCW has an ultra-wide operating bandwidth (the relative bandwidth is 28.71%) with its peak transmission efficiency higher than 90%.

B. FABRICATION AND EXPERIMANTAL VERIFICATIONS OF DOUBLE Y-SHAPED MPC CIRCULATOR

The sectional view of MPC circulator sample and the experimental setups for validating the MPC circulator are shown in Fig. 15. A precision-machined aluminum metal waveguide is used to fix the Al_2O_3 rods, while the central ferrite posts and pedestals are glued to the baseplate as shown in Fig. 15(a). The rubber plate absorbing materials mentioned above are also set around the Al_2O_3 rods arrays to absorb noise in the rhombic aluminous waveguide. In Fig. 15(b), the two ports of network analyzer link to the port 1 and 2 of the MPC circulator through two waveguides to coaxial converters and a pair of SMA connectors in order to measure the transmission characteristics between the circulator's port

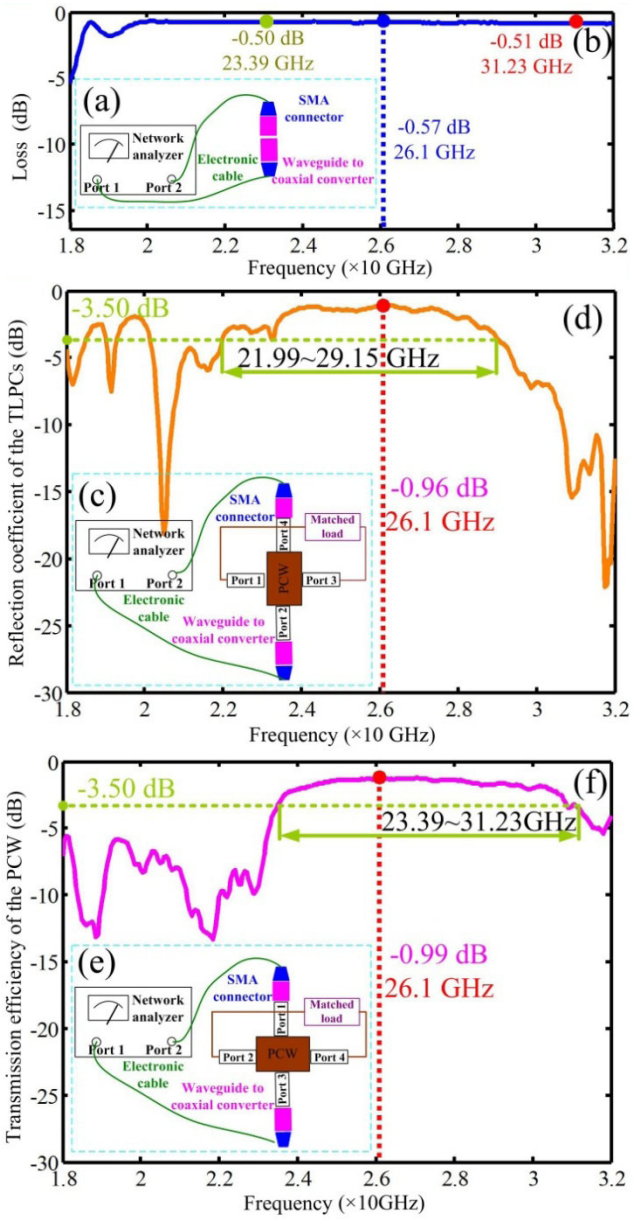

FIGURE 14. (a, c, e) The experimental setup for measuring the loss of the SMA connectors and waveguide to coaxial converters, the reflection coefficient of the TLPCs and the transmission efficiency of the PCW; (b, d, f) The corresponding results for (a, c, e).

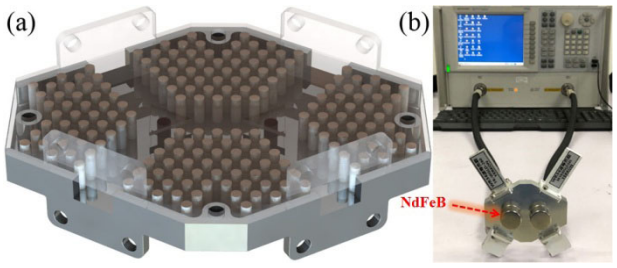

FIGURE 15. (a) Fabrication of four ports double Y-shaped MPC circulator; (b) Experimental setup for measuring the transmission characteristics of the MPC circulator.

1 and port 2. The other two ports 3 and 4 are connected to the WR34 matched loads.

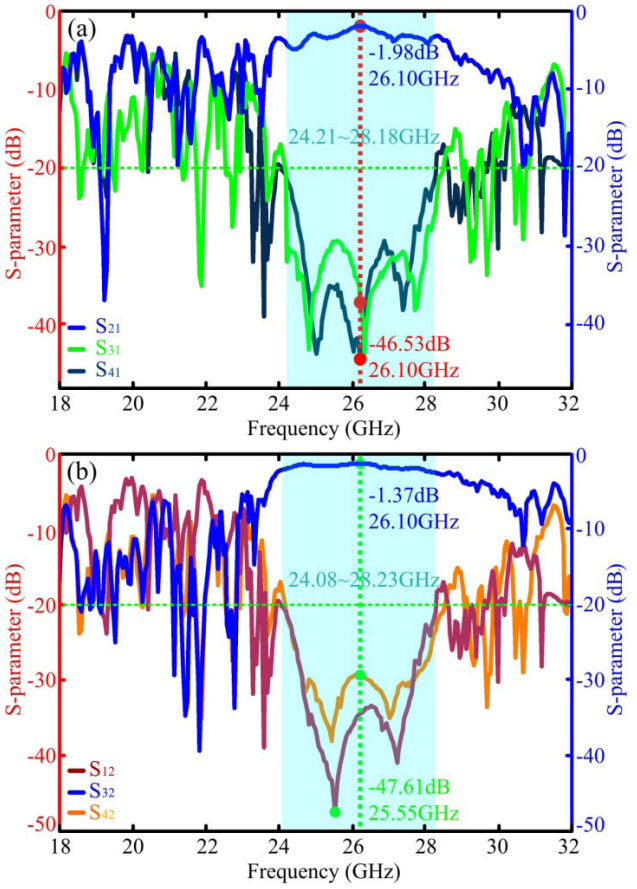

FIGURE 16. The measured insertion loss and isolation with frequency: (a) Electromagnetic waves launched from port 1 transmitting to port 2; (b) Electromagnetic waves launched from port 2 transmitting to port 3.

If the insertion loss from the electric cables is ignored, the insertion loss α_{21} and the isolation τ_{12} of the circulator shall be:

$$\alpha_{21} = -(S_{21} - \alpha_1) = \alpha_1 - 10\lg(P_{21}/P_1), \quad (14)$$

and

$$\tau_{12} = -S_{12} = -10\lg(P_{12}/P_2). \quad (15)$$

When signal is input into Port 1 of the circulator, its power is transmitted almost entirely to Port 2. When the ferrite posts are fully magnetized by NdFeB permanent magnets, the insertion loss and isolation are measured at the frequency region of 18 to 32 GHz, as shown in Fig. 16(a). The lowest insertion loss α_{21} is 1.41 dB (1.98 – 0.57dB) at 26.10 GHz, while the optimal isolation τ is 46.53 dB for port 4 to port 1. The bandwidth of the circulator covers from 24.21 to 28.18 GHz (the relative bandwidth is about 15.16%), which requires the isolation above 20 dB. Significantly, the measured bandwidth of the circulator under this transmission path, agree with the numerical value in Fig. 9(a). However, there are three peak values both for the measured isolation's curves of port 4 and port 3 to port 1. The possible reason is that the electromagnetic waves launched from Port 1 need to pass

through two ferrite regions with four ferrite posts to reach port 2. The incomplete symmetry of the ferrite posts' position lead the circulator's isolation to have more than three or even four peaks, which caused by the placement of the ferrite posts not accurate enough in the fabrication process.

Similarly, when signal is launched from port 2 of the circulator, the power is transmitted to port 3 and the other two ports are isolated. The measured insertion loss and isolation with frequency for the designed MPC circulator are shown in Fig. 16(b). The lowest insertion loss α_{32} is 0.80 dB (1.37 – 0.57dB) at 26.10 GHz, while the optimal isolation τ is 47.61 dB at 25.55 GHz for port1 to port 2. The bandwidth of the circulator covers from 24.08 to 28.23 GHz (the relative bandwidth is about 15.87%), which also requires the isolation above 20 dB. Different from the above, there are only two peaks for the isolation because the electromagnetic waves just only need to pass one ferrite region (two ferrite posts) under this transmission path. Similar calculated results and experimental phenomena have been reported in the literature [28].

Obviously, the relative bandwidth of the circulator in Fig. 16(b) is about 15.87% that only reaches wideband level in this experiment, but not up to the ultra-wideband level in Fig. 9(b) in calculation. The possible reasons are as follows: on the one hand, the placement precision for the ferrite posts' position and triangular pedestal is not enough to achieve perfect impedance matching in the circulator sample, which leads to the experimental bandwidth narrower than the numerical result; on the other hand, the relative permittivity of the Al_2O_3 rods is slight smaller than 9.2 in result the experimental bandwidth of the PCW in Fig. 14(f) is narrower than the calculated value in Fig. 6, which indirectly affects the bandwidth of the MPC circulator.

From the measurement results in Fig. 16, there are multiple dips in the isolation results indicating multiple modes or resonance are probably introduced inside the circulator which greatly increase its relative bandwidth. The physical mechanism for this great improvement of bandwidth is that the center frequencies of resonance of the four ferrite posts are slightly shifting each other and the frequencies are determined by machining accuracy of ferrite posts and their accuracy of the placement positions. The shifting each other may obtain multiple dips in the isolation results and the broadening of the bandwidth will degrade the isolation and insertion loss. The final overall results of the designed circulator' isolation in Fig. 16 is the superimposition of the different isolations from multiple resonances of different ferrite posts. The external matching broadening method mentioned in section D of part II based on the superimposition are widely applied for waveguide circulators' band broadening referring to [24] and [25].

The designed plans in [13] and [14] do not consider the circulators' band broadening. Only one cylindrical resonator formed by one cylindrical ferrite is studied in their circulator's junctions but the impedance matching between the junction cavity and the ports of the circulators are not considered. So there is only one high peak of isolation for their circulators, which can reach to be 60dB above whether in simulation or experiment. But the relative bandwidth of their circulators' are both narrow.

IV. CONCLUSION

A novel four ports double Y-shaped MPC circulator with ultra-wideband is proposed and first fabricated at 5G millimeter waveband in this paper. Through the numerical simulation on the relationship between the transmission efficiency of the PCW with its size in 3-D model, the optimal PCW structure with high transmission efficiency 90.78% is designed and validated at K-Ka band. Based on the high transmission PCW and gyromagnetic ferrite posts, the relative bandwidth of the designed MPC circulator is broadened to be ultra-wideband level of 28.48% by using EMBM in the numerical simulations. Due to the fabrication precision and material's problem, the relative bandwidth of our circulator sample only achieves 15.87% in the corresponding experiments.

As to the MPC circulator scheme it should be noted that the process is relatively simple and the materials can be obtained easily. If the problems that affect the working bandwidth mentioned above can be properly solved in engineering, our designed scheme of MPC circulator with low loss and easy integration not only can reduce light intensity to avoid nonlinear effect for integrated optical circuit in optical waveband, but also has potential applications in 5G communication systems due to its ultra-wideband characteristic from 24 to 28 GHz.

REFERENCES

[1] P. Pintus, D. Huang, C. Zhang, Y. Shoji, T. Mizumoto, and J. E. Bowers, "Microring-based optical isolator and circulator with integrated electromagnet for silicon photonics," *J. Lightw. Technol.*, vol. 35, no. 8, pp. 1429–1437, Apr. 15, 2017.
[2] P. Pintus, F. Di Pasquale, and J. E. Bowers, "Integrated TE and TM optical circulators on ultra-low-loss silicon nitride platform," *Opt. Express*, vol. 21, no. 4, pp. 5041–5052, Feb. 2013.
[3] E. J. Denlinger, "Design of partial height ferrite waveguide circulators," *IEEE Trans. Microw. Theory Techn.*, vol. MTT-22, no. 8, pp. 810–813, Aug. 1974.
[4] S. W. Y. Mung and W. S. Chan, "Active three-way circulator using transistor feedback network," *IEEE Microw. Wireless Compon. Lett.*, vol. 27, no. 5, pp. 476–478, May 2017.
[5] S. Wang, C.-H. Lee, and Y.-B. Wu, "Fully integrated 10-GHz active circulator and quasi-circulator using bridged-T networks in standard CMOS," *IEEE Trans. Very Large Scale Integr. Syst.*, vol. 24, no. 10, pp. 3184–3192, Oct. 2016.
[6] S. A. Oliver, P. M. Zavracky, N. E. McGruer, and R. Schmidt, "A monolithic single-crystal yttrium iron garnet/silicon X-band circulator," *IEEE. Microw. Guided Wave Lett.*, vol. 7, no. 8, pp. 234–239, Aug. 1997.
[7] Y. Akaiwa, "Operation modes of a waveguide Y circulator," *IEEE Trans. Microw. Theory Techn.*, vol. MTT-22, no. 11, pp. 954–960, Nov. 1974.
[8] T. Qiu, J. Wang, Y. Li, and S. Qu, "Circulator based on spoof surface plasmon polaritons," *IEEE Antennas Wireless Propag. Lett.*, vol. 16, pp. 821–824, 2016.
[9] E. Yablonovitch, "Inhitited spontaneous emission in solid-state physics and electronics," *Phys. Rev. Lett.*, vol. 58, pp. 2059–2062, May 1987.
[10] S. John, "Strong localization of photons in certain disordered dielectric super-lattices," *Phys. Rev. Lett.*, vol. 58, pp. 2486–2489, Jun. 1987.
[11] Z. Wang and S. Fan, "Optical circulators in two-dimensional magneto-optical photonic crystals," *Opt. Lett.*, vol. 15, pp. 1989–1991, Aug. 2005.
[12] V. Dmitriev, M. N. Kawakatsu, and F. J. M. de Souza, "Compact three-port optical two-dimensional photonic crystal-based circulator of *W*-format," *Opt. Lett.*, vol. 37, no. 15, pp. 3192–3194, Aug. 2012.

[13] F. Fan, S.-J. Chang, C. Niu, Y. Hou, and X.-H. Wang, "Magnetically tunable silicon ferrite photonic crystals for terahertz circulator," *Opt. Commun.*, vol. 285, no. 18, pp. 3763–3769, Aug. 2012.
[14] Y. Wang, D. Zhang, S. Xu, B. Xu, Z. Dong, and Q. Xue, "Microwave-frequency experiment validation of a novel magneto-photonic crystals circulator," *IEEE Photon. J.*, vol. 10, no. 3, Feb. 2018, Art. no. 5300106.
[15] Y. Wang, D. Zhang, S. Xu, B. Xu, and Z. Dong, "H-plane cross-shaped waveguide circulator in magneto-photonic crystals with five ferrite posts," *Chin. Opt. Lett.*, vol. 15, no. 10, pp. 1116011-1–1116011-4, Nov. 2017.
[16] D. S. Sundar, C. Umamaheswari, T. Sridarshini, M. Karthikeyan, R. Sitharthan, A. S. Raja, and M. F. Carrasco, "Compact four-port circulator based on 2D photonic crystals with a 90° rotation of the light wave for photonic integrated circuits applications," *Laser Phys.*, vol. 29, no. 6, p. 066201, Jun. 2019.
[17] L. Zhao, Z.-M. Chen, and J. Wang, "A wideband dual-polarized omnidirectional antenna for 5G/WLAN," *IEEE Access*, vol. 7, pp. 14266–14272, 2019.
[18] B.-J. Wen, L. Peng, X.-F. Li, K.-S. Mo, X. Jiang, and S.-M. Li, "A low-profile and wideband unidirectional antenna using bandwidth enhanced resonance-based reflector for fifth generation (5G) systems applications," *IEEE Access*, vol. 7, pp. 27352–27361, Mar. 2019.
[19] M. H. Dahri, M. H. Jamaluddin, M. Inam, and M. R. Kamarudin, "A review of wideband reflectarray antennas for 5G communication systems," *IEEE Access*, vol. 5, pp. 17803–17815, Aug. 2017.
[20] G. R. Maccartney, T. S. Rappaport, S. Sun, and S. Deng, "Indoor office wideband millimeter-wave propagation measurements and channel models at 28 and 73 GHz for ultra-dense 5G wireless networks," *IEEE Access*, vol. 3, pp. 2388–2424, 2015.
[21] W. El-Halwagy, R. Mirzavand, J. Melzer, M. Hossain, and P. Mousavi, "Investigation of wideband substrate-integrated vertically-polarized electric dipole antenna and arrays for mm-wave 5G mobile devices," *IEEE Access*, vol. 6, pp. 2145–2157, 2018.
[22] Y. Zhou, F. Zhu, S. Gao, Q. Luo, L.-H. Wen, Q. Wang, X. Yang, Y. Geng, and Z. Cheng, "Tightly coupled array antennas for ultra-wideband wireless systems," *IEEE Access*, vol. 6, pp. 61851–61866, Nov. 2018.
[23] E. H. Mujammami and A. B. Sebak, "Wideband high gain printed Quasi-Yagi diffraction gratings-based antenna for 5G applications," *IEEE Access*, vol. 7, pp. 18089–18100, 2019.
[24] W. S. Piotrowski and J. E. Raue, "Low-loss broad-band EHF circulator," *IEEE Trans. Microw. Theory Techn.*, vol. 24, no. 11, pp. 863–866, Jan. 2003.
[25] D.-G. Zhang and E. K.-N. Yung, "Investigation of waveguide Y-junction circulator with a triangular ferrite post," *Int. J. Infr. Millim. Waves*, vol. 21, no. 1, pp. 123–131, Jan. 2000.
[26] E. K. N. Yung, D. G. Zhang, and R. S. K. Wong, "A novel waveguide Y-junction circulator with a ferrite sphere for millimeter waves," *IEEE Trans. Microw. Theory Techn.*, vol. 44, no. 3, pp. 454–456, Mar. 1996.
[27] Z. Dengguo and L. Weigan, "A new design method of H-plane waveguide circulator," *Int. J. Infr. Millim. Waves*, vol. 9, no. 2, pp. 173–177, Nov. 1988.
[28] W. B. Dou and Z. L. Sun, "Millimeter wave ferrite circulators and rotators," *Int. J. Infr. Millim. Waves*, vol. 17, no. 12, pp. 2035–2131, Dec. 1996.

YONG WANG was born in Hubei, China. He received the M.S. and Ph.D. degrees in optics and optical engineering from Shenzhen University, Shenzhen, China, in 2014 and 2018, respectively. After graduation, he is currently a Postdoctoral Researcher with the Shenzhen Key Laboratory of Micro-Nano Photonic Information Technology, College of Physics and Optoelectronic Engineering, Shenzhen University. His research interests include magneto-photonic crystal devices and antennas.

DENGGUO ZHANG was born in Sichuan, China. He received the B.Eng. and Ph.D. degrees in electrical engineering from the University of Electronic Science and Technology of China, in 1983 and 1988, respectively. After graduation, he was with the Institute of Electromagnetic and Microwave Technology, Southwest Jiaotong University, Chengdu, China. He was with the Department of Electronic Engineering, City University of Hong Kong, for two years. He taught at Shenzhen University after April 1995 and was promoted to Professor at the end of 1997. He is currently with the College of Electronics and Information Technology, Shenzhen University, China. His research interests include wireless communications, microwave and RF circuit and devices, millimeter-wave techniques, waveguide circulator, and magneto-photonic crystal devices.

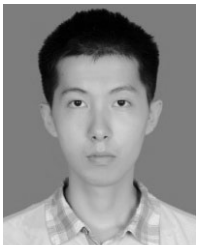

BIAOGANG XU was born in Guangdong, China. He received the B.Eng. degree in mechatronic engineering from the Zhongkai Institute of Agricultural Engineering. He is currently pursuing the Ph.D. degree in optical engineering with the College of Physics and Optoelectronic Engineering, Shenzhen University, Shenzhen, China. His research interests include magneto-photonic crystals' devices and antennas.

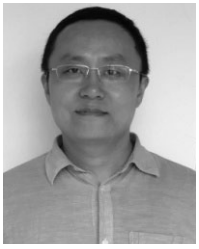

ZHENG DONG was born in Jiangsu, China. He received the B.S. degree in electronic engineering from the University of Hangzhou Electronic Science and Technology, Hangzhou, China, in 2002. He is currently pursuing the M.S. degree with the College of Electronics and Information Technology, Shenzhen University, China. He was the Director of Green Tech Corporation, China. His research interests include antennas and magneto-photonic crystals' devices.

XUANKE ZENG was born in Guangdong, China. He received the M.S. and Ph.D. degrees in optics and optical engineering from Shenzhen University, Shenzhen, China, in 2013 and 2016, respectively, where he is currently a Postdoctoral Researcher with the Shenzhen Key Laboratory of Micro-Nano Photonic Information Technology, College of Physics and Optoelectronic Engineering. His research interests include ultrafast optics and ultrafast imaging.

JIHONG PEI was born in Gansu, China. He received the Ph.D. degree from the Xi'an University of Electronic Science and Technology, in 1998. From 1989 to 2002, he was with the Xi'an University of Electronic Science and Technology. He has been with Shenzhen University, since 2002. He is currently the Director of the Department of Electronics, School of Information Engineering, Shenzhen University, and the ATR National Defense Science and Technology Key Laboratory, Shenzhen University. His main research interests include image and video content analysis, intelligent video surveillance, multi-camera panoramic video technology, pattern recognition and machine learning, multi-spectral remote sensing image analysis, vector field signal, and image analysis. He is a member of the China Aeronautical Member Information Fusion Branch.

SHIXIANG XU received the Bachelor of Optical Instruments degree from Zhejiang University and the Ph.D. degree from the Shanghai Institute of Optical Precision Machinery, Chinese Academy of Sciences. He was a Postdoctoral and a Visiting Scholar in USA, France, Germany, and other countries. He was selected as Pujiang talents in Shanghai, in 2006, and was funded by the Ministry of Education, in 2007. He was transferred to Shenzhen University from East China normal University, in June 2008. He is currently a Professor and a Doctoral Supervisor with the Shenzhen Key Laboratory of Micro-Nano Photonic Information Technology, College of Physics and Optoelectronic Engineering, Shenzhen University. His research interests include ultra-fast optics, all-solid-state laser technology, ultra-short pulse laser technology, ultra-fast imaging, and pulse terahertz optics.

QUAN XUE (M'02–SM'04–F'11) received the B.S., M.S., and Ph.D. degrees in electronic engineering from the University of Electronic Science and Technology of China (UESTC), Chengdu, China, in 1988, 1990, and 1993, respectively. In 1993, he joined the UESTC as a Lecturer and became an Associate Professor, in 1995, and then a Professor, in 1997. From October 1997 to October 1998, he was a Research Associate and a Research Fellow with The Chinese University of Hong Kong. In 1999, he joined the City University of Hong Kong, where he was a Chair Professor of microwave engineering. He is currently the Dean of the School of Electronic and Information Engineering, South China University of Technology, Guangzhou, China. His research interests include wireless communications, microwave and RF circuit and subsystems, millimeter-wave techniques, microwave monolithic integrated circuits, and antennas.